

The following supplements accompany the article

Functional morphology of the flounder allows stable and efficient gliding: an integrated analysis of swimming behaviour

Tsutomu Takagi^{1,*}, Ryo Kawabe², Hiroyuki Yoshino³, Yasuhiko Naito⁴

¹Faculty of Agriculture, Kinki University, Nara 631-8505, Japan

²Institute for East China Sea Research Centre, Nagasaki University, Nagasaki 851-2213, Japan

³Hokkaido Industrial Technology Centre, Hakodate 041-0801, Japan

⁴National Institute of Polar Research, Tokyo 173-8515, Japan

*Corresponding author. Email: tutakagi@nara.kindai.ac.jp

Aquatic Biology 9: 149–153 (2010)

Supplement 1. Supplementary information to Materials and methods

FIELD EXPERIMENTS AND DATA LOGGERS

Released individuals and release site. During October and November 2000, the swimming behaviour of adult Japanese flounder *Paralichthys olivaceus* was studied off the coast of the Tsugaru Strait on the southern coast of Hokkaido, Japan (Fig. S1). All flounders were caught in set-nets or by hook in Kikonai Bay and then retained in a circular holding tank (5 m diameter, 0.5 m depth). The water temperature in the holding tank was maintained at ambient ocean temperature (approximately 14°C); natural light cycles were also simulated. Twenty-one flounders were selected for tagging. The flounders were released on 3 different dates: 3 with a PD2G logger and 6 with a DT logger on 21 October, 1 with a PD2G logger and 4 with a DT logger on 28 October, and 6 with a PD2G logger and 1 with a DT logger on 11 November 2000 (Kawabe et al. 2004). After capture, the tagged flounders were retained in the holding tank for 2 to 4 d before being released.

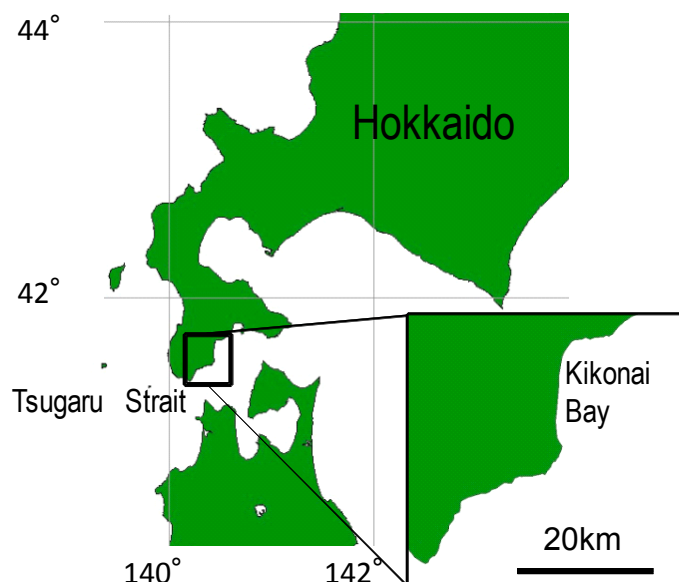


Fig. S1. Field experiment site in Kikonai Bay off the southern coast of Hokkaido

Specifications of the data loggers. The PD2G logger (Little Leonard) is cylindrically shaped (2 cm diameter, 12 cm length) with a weight of 60 g in air and 22 g in seawater. This logger is capable of recording swimming speed and depth at 1 or 0.5 s intervals, and heave and surge

accelerations at 0.063 and 0.25 s intervals, respectively. The maximum depth that could be measured was 190 m with a resolution of 0.05 m. The measuring range of the acceleration was $\pm 40 \text{ m s}^{-2}$ with a resolution of 0.02 m s^{-2} . The body angle was calibrated while flounder with an attached PD2G logger were placed on a horizontal surface.

The DT logger (Little Leonard) is cylindrical (1 cm diameter, 8 cm length) with a weight of 27 g in air and 5 g in seawater. Depth recordings were conducted at 3 s intervals. The resolution of the depth sensor was 0.4 m. The maximum permissible depth was 100 m (Kawabe et al. 2004).

Procedures for attachment of loggers and the resulting effect on the flounder. Flounders were anaesthetized by briefly submerging them in well-oxygenated seawater containing 0.3 ml^{-1} 2-phenoxyethanol. Data loggers were then attached such that they were aligned with the longitudinal body axis on the ocular side (Fig. S2). To prevent the data logger from inhibiting the manoeuvrability of the fish, it was positioned such that the effect on the moment of inertia of the flounder was minimized. Thin plastic strings were used to attach the loggers to the fish. This attachment method required that the body be penetrated. Consequently, the logger had to be positioned at a location near the centre of gravity of the flounder where the thickness of the body (at the incision site between the side fin and the spine) was not great. The centre of gravity of the flounders was located at approximately 0.4 total length (TL) from the snout. A logger was attached to the anterior muscular region between the longitudinal body axis and the dorsal fin. The strings that held the logger were passed through 2 holes (1 mm diameter) and secured to a rubber disc on the blind side of the fish. Flounders were retained for at least 24 h in the holding tank to allow recovery after this incision surgery. Following recovery, fish were transferred by boat to water at a depth of 20 m—a journey that took 20 min from the holding tank—and released.

We previously conducted experiments to investigate the effects of this instrumentation on the behaviour of flatfish. The swimming speed and tail-beat frequency of flounder with attached loggers was 0.5 to 1.5 body lengths (BL) s^{-1} and 1.2 to 2.4 Hz, respectively; however, the fish rarely swam over 1.2 BL s^{-1} . There was no observed difference in swimming speed and tail-beat frequency between flatfish with and without attached loggers (Kawabe et al. 2003, 2004).

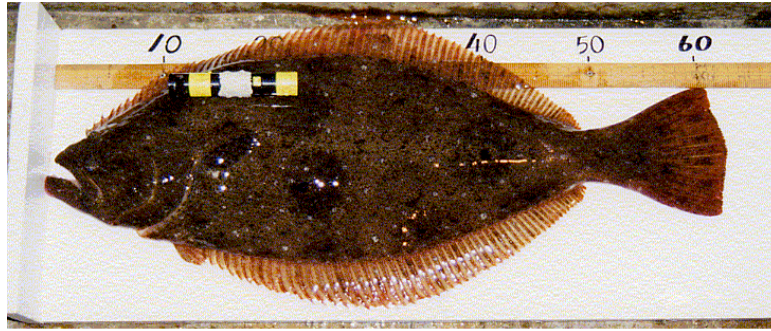


Fig. S2. *Paralichthys olivaceus*. Flounder with attached PD2G logger on the ocular side

Swimming and gliding measurements using loggers

Detection of tail beating and the body angle of flounders. The accelerometer in the PD2G logger can detect accelerations in 2 directions: surge acceleration, which occurs along the longitudinal body axis, and heave acceleration, which occurs perpendicular to the surge direction from the ocular and blind sides (Fig. S3). Tail-beat oscillations were detected from the remaining high frequency data extracted through a 0.1 Hz high-pass filter (IFDL version 3.1, WaveMetrics) from the heave acceleration time-series data.

Since the gravity component is the trigonometric function of the tilt-angle of the acceleration (surge direction) sensor, the component can be transformed into the body angle based on the calibration result. The horizontal position of the tagged flounders was determined by placing the fish on a horizontal surface.

The sensor for surge acceleration measured the acceleration with respect to changes both in the movements of flounder and in gravitational acceleration. Therefore, the body angle during movement was obtained from the acceleration due to gravity, which was the low frequency data separated from the time-series of surge acceleration using a low-pass filter (IFDL version 3.1, WaveMetrics) (Kawabe et al. 2003, 2004). The low-pass filter characteristics for Japanese flounder are less than 0.4 Hz, which seems to be sufficiently low to remove tail-beat frequencies.

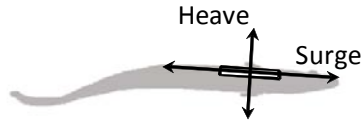


Fig. S3. Heave and surge acceleration detected by a logger attached to the flounder body surface

Glide speed and angle during gliding. Fig. S4 is a schematic view of a flounder during gliding, showing the glide speed, body angle, glide angle, and angle of attack during gliding.

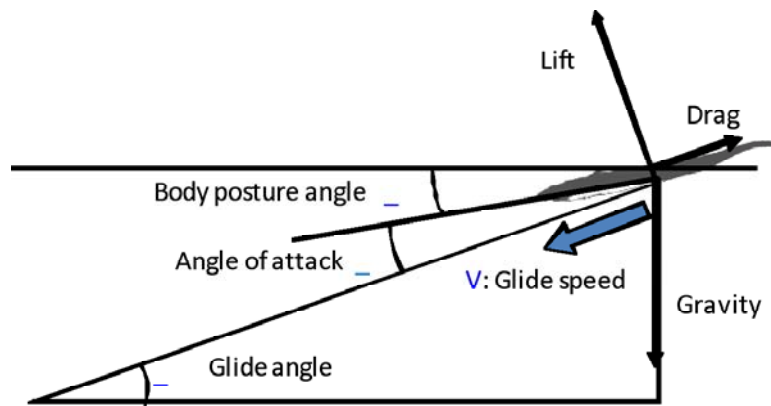


Fig. S4. A schematic view of a flounder showing the parameters measured during a steady glide

Glide speed is defined as the speed through the water (rather than the speed over the seabed). The actual glide speed in the field data was measured using a rotating turbine. The theoretical speed can be estimated from Eq.(2) in the main text. Swimming speed is the speed thorough the water during both gliding and powered swimming. Flow speed is the speed (as mentioned in (Eq. (3) and (4) the main text) of the steady flow in the domain for the computational fluid dynamics (CFD) analysis. A steady flow has to be run into the inlet so that the model of the flounder was set in the domain.

The effect of current flow on the data measured by the logger. Current flow obviously occurs everywhere in the field. An object in the sea will be moved by the current such that a state of mechanical equilibrium is reached. Thus a flounder in the field should be moved if a current flow is present. However, note that a logger attached to the flounder can measure the flow speed and the body angle in the Lagrangian representation on the coordinate system relative to the body, not global coordinates. This shows that a horizontal steady current flow does not affect the measurement of the body angle, nor does it affect the turbine or the depth sensor of a logger fixed on a gliding flounder because the flounder moves with the current.

Unsteady motion caused by turbulence in the current flow will not affect the measurements because the current flow has spatio-temporal uniformity for short time durations such as gliding time. The flounder accelerates when it commences and ends gliding, but the unsteady motion is a variation that occurs for a very short time until a state of mechanical equilibrium is again reached.

Vertical flow in the sea can be caused by waves on the free surface. However, as the vertical velocity should decay exponentially with depth and the swimming depth of flounder almost always exceeds 10 m, the effect of the vertical flow appears to have little influence on the parameters measured during gliding. If the depth sensor could detect vertical flow due to waves or other effects, the most frequent value of the sinking rate of flounders in the field data (Fig. 2a in the main text) would not agree with the theoretical value.

Modelling of the flounder and theoretical calculations

Modelling of the flounder. We constructed a model flounder, the TL and height of which were 60 and 26 cm, respectively (Fig. S5). The model had almost the same total length and height as flounders A1 and A2.

In order to scan individuals accurately, we have to use dimensions smaller than 60 cm. Therefore, to investigate the morphological similarity of different-sized flounders, we examined the relationships between TL and total height (TH, cm), TL and total width (TW, cm), and total length and the projected area of the ocular side (A_o , cm²) in 18 flounders which ranged from 33 to 69 cm TL.

The results were as follows:

best-fitting linear regression between TL and TH:

$$TH = 0.52 TL - 5.2, r^2 = 0.95, p < 0.001,$$

best-fitting linear regression between TH and TW:

$$TW = 0.12TL - 1.81, r^2 = 0.91, p < 0.001$$

best-fitting linear regression between TL and A_0 :

$$A_0 = 0.26TL^{2.0}, r^2 = 0.99, p < 0.001$$

On the basis of the above results, we can assume that the morphologies of mature flounders are similar even though their sizes may differ.

In order to achieve accurate scanning, we have to reduce the size of the body without bending it; therefore, we should use an individual of 33 cm TL for scanning and an individual of 60 cm TL for the CFD modelling, corresponding to the size range of the individuals used in the field experiment.

In a previous study, we observed that the body was almost flattened during gliding (Kawabe et al. 2003). Thus when scanning individuals, to eliminate the effect of gravity and any deformation of the individual, an individual with flattened post-mortem rigidity was suspended by a fine nylon line.

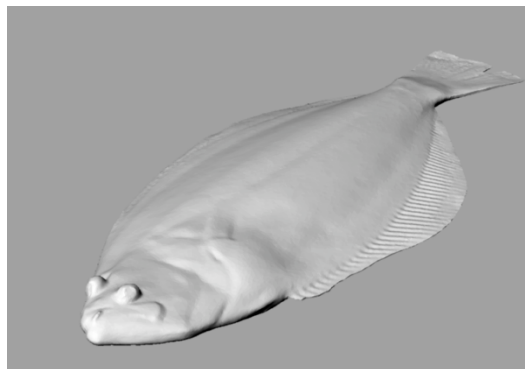


Fig. S5. The 3-dimensional (3D) surface profile of the flounder produced by a 3D non-contact surface profiler. The total length and weight of the fish were 60 cm and 2.2 kg, respectively

CFD software and the finite volume method. SCRYU/Tetra (Software Cradle) is an all-in-one CFD software package using an unstructured mesh and the finite volume method. The application of this software can yield precise shape reproduction for effective results, and can therefore be used to evaluate the fluid dynamics around the bodies of living organisms.

The finite volume method was developed as a CFD method and uses the integral form of the conservation equations. The solution domain is subdivided into a finite number of contiguous control volumes, which are unstructured grids such as prisms, triangles, or

tetrahedrons. Therefore, it can accommodate any type of grid and is suitable for analysing complex geometries.

As the differential form of the governing equations is integrated over the control volume, the resulting solution satisfies the conservation of physical quantities such as mass, momentum, and energy. At present, it is one of the most versatile discretisation techniques available in commercial CFD software (Ferziger & Peric 1999).

Computation conditions. The nearer the grid is to the body, the finer it is. This can make the computational effort more efficient, and also enables a precise estimate of the fluid structure and pressure around the body.

The prism layer, which is in contact with the body, was 2.2×10^{-4} m thick. The grid size, which was located far off, was approximately 8×10^{-2} m. There were 3500000 elements in the calculation domain.

The boundary condition on the surface of the rectangular calculation domain was free-slip, but no-slip and no-flux boundary conditions on the body surface are required.

The simulations ran for 6 to 12 h before reaching a steady state. The simulations were run using an Intel 2.8 GHz Xeon Processor with 2 GB memory.

When variation in the velocity components (V_x , V_y , V_z) and the pressure in each element were less than 0.0001, we considered that the flow field around the model had attained a steady state. Under this convergence condition the simulated time to reach steady state from rest was 8.6 to 15.6 s at angles of attack of 2 and 20°, respectively.

Supplement 2. Supplementary information to the results

FIELD EXPERIMENT

The total length, body weight, and duration of data logging for each retrieved Japanese flounder *Paralichthys olivaceus* are shown in Table S1. Table S2 shows the number of glides, glide height, glide duration, and sink rate of each retrieved flounder.

Table S1. *Paralichthys olivaceus*. Total length, body weight, and duration of data logging for the 8 retrieved flounder specimens

Flounder no.	Tag	Total length (cm)	Body weight (kg)	Record duration (d)
A1	PD2G	60.6	2.2	1.4
A2	PD2G	60.6	2.2	5.2
D1	DT	51.8	1.4	24.3
D2	DT	51.6	1.3	6.2
D3	DT	57.4	1.7	25.0
D4	DT	63.4	2.4	25.3
D5	DT	52.6	1.4	7.1
D6	DT	50.2	1.2	14.2

Table S2. *Paralichthys olivaceus*. Number of glides, glide height, glide duration, and rate of sinking (S_R) for each flounder. As the DT logger cannot detect tail beating, we defined a gliding descent of individuals tagged with DT loggers as downward movement at a nearly constant rate of sinking from over 2 m above the seabed. Specimen D3 was detected moving away from the seabed by more than 2 m on only 2 occasions; consequently, the data for this individual was excluded

Flounder no.	No. glides	Average glide height (m)	Average glide duration (s)	S_R (cm s^{-1})
A1	35	1.4 ± 1.5	10 ± 9	12.8 ± 8.5
A2	115	1.7 ± 1.9	24 ± 38	8.4 ± 2.1
D1	62	4.2 ± 2.7	39 ± 29	12.9 ± 6.8
D2	26	4.8 ± 2.9	40 ± 30	13.8 ± 5.0
D4	104	4.1 ± 2.7	54 ± 32	9.8 ± 7.4
D5	61	3.8 ± 1.8	50 ± 20	7.7 ± 1.7
D6	51	4.0 ± 2.1	45 ± 26	10.5 ± 6.4

Theoretical calculation

Flow field around a modelled flounder. The flow field around the model at an angle of attack of 0° is shown in Fig. S6. Fig. S7 shows the flow field from the anterior side to illustrate the transverse flow that arises on the ocular side. Twin-bound vortex flows occur at both side fins because circulation flow is generated around an aerofoil in steady flow. The bound vortex flow may interfere with the flow entering the turbine, preventing the accurate measurement of the flow speed. In addition, when a calibration test was carried out to check the rotation of the turbine in a flume tank, foreign objects occasionally prevented the turbine from rotating smoothly. These effects may have contributed to an underestimation of the flow speed in the field data.

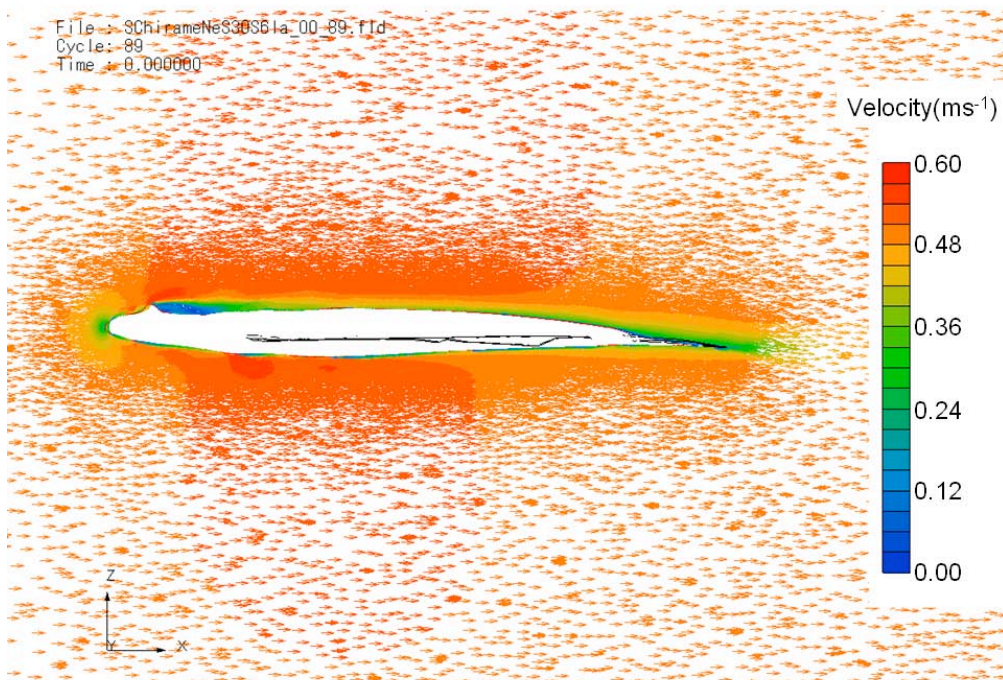


Fig. S6. Velocity field structure around the flounder at an angle of attack of 0° calculated using the computational fluid dynamics program. Arrows show the direction of flow and the colours are proportional to the magnitude of flow

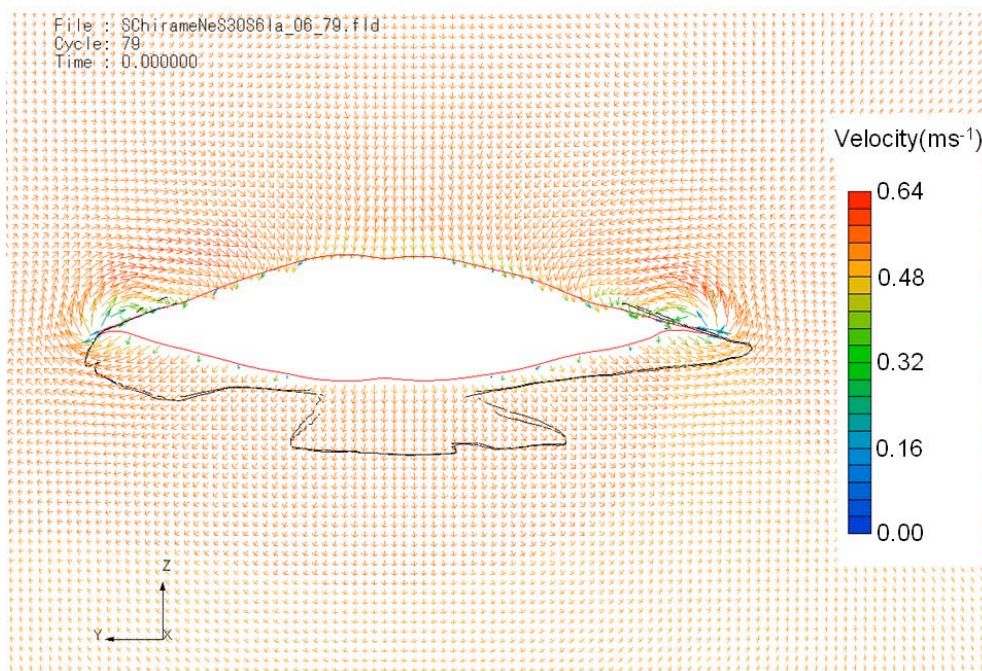


Fig. S7. Flow field from the anterior side of the flounder at an angle of attack of 6°. Arrows show the direction of flow and the colours are proportional to the magnitude of flow

LITERATURE CITED

- Ferziger JH, Peric M (1999) Computational methods for fluid dynamics. Springer, Berlin
- Kawabe R, Naito Y, Sato K, Miyashita K, Yamashita N (2004) Direct measurement of the swimming speed, tailbeat, and body angle of Japanese flounder (*Paralichthys olivaceus*). ICES J Mar Sci 61:1080–1087
- Kawabe R, Nashimoto K, Hiraishi T, Naito Y, Sato K (2003) A new device for monitoring the activity of freely swimming flatfish, Japanese flounder *Paralichthys olivaceus*. Fish Sci 69:3–10